Available online at www.sciencedirect.com
ScienceDirect
Journal of Power Sources 172 (2007) 877–885
JOURNAL OF POWER SOURCES
www.elsevier.com/locate/jpowsour

Vanadium diphosphides as negative electrodes for secondary Li-ion batteries

F. Gillot [a], M. Ménétrier [b], E. Bekaert [b], L. Dupont [a], M. Morcrette [a], L. Monconduit [c,*], J.M. Tarascon [a]

[a] *LRCS-UMR 6007, Université de Picardie Jules Verne, F80039 Amiens, France*
[b] *ICMCB-ICMCM-CNRS, F33608 Pessac, France*
[c] *LAMMI-UMR 5072, Université Montpellier II, F34095 Montpellier, France*

Received 13 December 2006; received in revised form 14 May 2007; accepted 15 May 2007
Available online 21 May 2007

Abstract

We report on the Li electrochemical reactivity of amorphous and crystalline VP_2, synthesized by ball-milling and by 600 °C heat treatment of a ball-milled sample, respectively. The amorphous sample can reversibly react with 3.5 Li per formula unit as compared to solely 2.5 for the crystalline one. However in both cases there is a rapid capacity decay upon cycling that is more pronounced in the case of the crystalline sample. Complementary X-rays, HTREM and NMR tend to show that the Li reactivity mechanism differs from the classical conversion reactions since neither V nanoparticles nor the formation of Li_3P were detected, as opposed to some of the other MP_2 compounds (M = Ni or Cu). Besides structural phase variations within the 3d metal-based binary phosphide series, the possibility of a change in the nature of the redox centre upon lithiation from cation (M) to anion (P) is evoked.

Keywords: Lithium ion batteries; Vanadium diphosphides; Ball-milling; Capacity retention

1. Introduction

Owing to the intrinsic limitation of classical insertion/de-insertion electrodes to about 1 electron per 3d-metal, there has been considerable interest in the search for alternative Li electrochemical reactivity mechanisms. Among them are the Li-driven displacement reactions in Cu-based compounds that are concomitant with a reversible Cu-extrusion-re-injection process [1,2], or the conversion reactions that can reversibly accommodate 2 or 3 electrons per 3d-metal compared to 1 for insertion reactions [3].

Conversion reactions are quite universal since they occur with oxides [4], sulphides [5], nitrides [6], fluorides [7] and phosphides [8]. Although quite attractive such reactions suffer from poor energetic yield owing to the unusual large polarization between charge and discharge, even at low currents. Such a polarization, which represents the threshold potential to ignite a conversion reaction, was shown to be strongly dependent on the nature of the anion within the precursor phase. It decreases as the electro-negativity of the anion decreases (e.g., in moving from fluorides to oxides, nitrides and phosphides), with the lowest values obtained for the phosphides.

In light of such correlation, research on ternary and binary phosphides has regained attention with the appearance of materials that can uptake large amounts of Li through mechanisms involving insertion, displacement or conversion reactions or combination of them. More specifically, some of the binary phosphides (FeP_2, NiP_2) were shown to reversibly uptake about 6Li per unit formula according to the overall reaction $MP_2 + 6Li^+ \rightarrow M + 2Li_3P$ resulting in large capacities (1000 mAh/g) at an average potential of about 1 V with a 0.4 polarization, with therefore poor power rate and capacity retention; especially for FeP_2 [8,9]. To address power rate limitations we have considered the direct growth of NiP_2 material onto Ni foam in order to enhance the current collector/NiP_2 interface and consequently both charge and mass transfers [8]. Achieving long-term stability has been more problematic owing to the partial electrochemical instability of Li_3P in the electrolytes. Hints

* Corresponding author. Tel.: +33 467 14 33 35; fax: +33 467 14 33 04.
E-mail address: Laure.monconduit@univ-montp2.fr (L. Monconduit).

0378-7753/$ – see front matter © 2007 Elsevier B.V. All rights reserved.
doi:10.1016/j.jpowsour.2007.05.043

of improvements were therefore noted by increasing the discharge cut-off voltage so as to limit the amount of Li_3P formed to the expense of a lowering of the electrode capacity. Moving along the same direction, we decided to search for phosphides that could react with Li through a conversion process enlisting less oxidized P_n^{x-} species (LiP, M–Li–P).

Surveys on 3d-metal oxides have shown that conversion reactions were most likely to occur with the late rather than with the early 3d-elements of the periodic table. With V-based oxides, we did not succeed in getting evidence of V nanoparticles in a fully reduced composite electrode [10]. Instead we showed a V–O–Li-type bonding. Previous studies on phosphides seem to indicate similar trends. The formation of Li_3P is, for instance, unambiguous with NiP_2 whereas it is debatable with FeP_2. Moreover, recent studies on V-based phosphides have failed to reveal the formation of Li_3P as well as that of V nanoparticles while such materials were shown to reversibly react with 7Li per formula unit [15,16]. Along that line of thinking, the VP_2 phase was quite appealing, hoping that it could uptake large amounts of Li like its counterparts FeP_2, NiP_2, without leading to the formation of Li_3P spotted as troublesome to achieve good cyclability. The core of the paper is the synthesis and structural characterization of VP_2 together with its electrochemical behaviour with respect to Li.

2. Experimental

2.1. XRD, TEM and SEM

X-ray diffraction (XRD) measurements on powdered VP_2 samples were performed on D8 Bruker X-ray diffractometer using the Co K_α radiation.

A specifically modified scanning electron microscope Philips field effect gun (FEG) XL-30, as previously reported [11], was used to carry out SEM studies on either Li-free or partially lithiated samples. Tecnai F20 ST transmission electron microscope equipped with EDS analysis was used to conduct our TEM/HRTEM investigations. To perform these experiments the cells were stopped and opened in a dry box once cycled down to the required voltage. The partially lithiated material was recovered and washed with dimethyl carbonate (DMC) prior to being placed onto a copper grid mounted on our TEM sample holder. Through a special mobile airlock of our own design, the sample was then transferred to the TEM, without any air exposure, for selected-area electron diffraction (SAED) pattern and bright field image collection.

2.2. Electrochemical tests

Swagelok-type cells were assembled in an argon-filled glove box and cycled using a VMP automatic cycling/data recording system (Biologic Co, Claix, France). These cells comprise a Li metal disc as the negative electrode, a Whatman GF/D borosilicate glass fibre sheet saturated with a 1 M $LiPF_6$ solution in ethylene carbonate (EC), dimethyl carbonate (DMC) (1:1 in weight) as the electrolyte, and unless otherwise specified, a positive electrode made by mixing the starting transition metal phosphides powder with 15% (weight) carbon black (SP). Usually, 10–12 mg of the mixed powders was placed on top of the Swagelok plunger. Electrochemical tests were realized using a potential window between 2 and 0.01 V versus Li^+/Li^0 and a cycling rate of C/10 (that is one lithium per formula unit in 10 h).

In situ XRD electrochemical cells assembled similarly to our Swagelok cell but with a beryllium window as current collector on the X-Ray side were placed on a Bruker D8 diffractometer (Co Radiation) equipped with a PSD detector, and connected to the VMP system. The cell was discharged at a C/10 rate and the X-ray powder patterns were collected for every 1 reacted 0.1Li.

2.3. XAFS spectroscopy

Measurements were performed at Daresbury Laboratory (Great Britain) on the 7.1 station that is designed and optimized for X-ray spectroscopy (XRS) or X-ray absorption fine structure (XAFS) studies in an energy range of 4–12 keV. Several spectra at ambient temperature were recorded on the V (5464 eV) edge for the starting materials as well as those prepared by lithium insertion. On a practical side, the air sensitive samples were assembled as polymer films in an argon-filled glove box. It consists in mixing a PVDF-HFP polymer dissolved in acetone, then spreading the solution, and letting it dry. The obtained film is heat-sealed in a blue waterproof aluminium bag.

2.4. NMR spectroscopy

^{31}P and ^{7}Li MAS NMR measurements were carried out with a Bruker Avance 300 spectrometer, using a standard Bruker 2.5 mm MAS probe, at a 30 kHz spinning speed. Materials recovered from positive electrodes were placed in the rotors in an Ar-filled glove box. For ^{31}P (121 MHz), a Hahn echo pulse sequence (with refocusing delay equal to one rotor period i.e. 33.3 μs) was used, the 90° pulse was 1.7 μs and the recycle delay was 60 s. The reference is H_3PO_4 (85%). For ^{7}Li experiments (116 MHz), a single pulse was used with a 2.2 μs 90° pulse and a 20 s recycle delay. The 0 ppm reference is LiCl 1 M in aqueous solution.

3. Results

3.1. Synthesis

The VP_2 phase is prepared by ball-milling vanadium (99%, Aldrich) and red phosphorous (Alfa Aesar, 100 mesh, 99%). To prevent the products from oxidizing, the experiments are carried out in an Ar-filled glove box. Stoichiometric amounts of the powdery elements are placed in a stainless steel reactor, which inside is coated with a tungsten carbide layer. The reactor is then placed onto a planetary grinder (Retsch 100) and the grinding is performed with 10 mm diameter stainless steel balls; the ball to powder weight ratio being equal to 10. After 50 h grinding at 600 rpm, the X-ray diffraction pattern, showing only one broad peak corresponding to the (1 1 1) reflection, reveals a

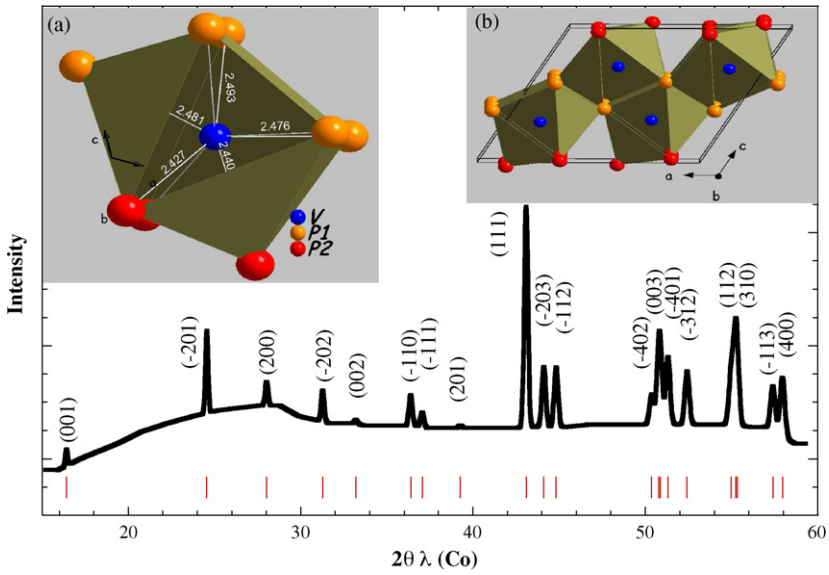

Fig. 1. X-ray diffraction patterns (Co K_α) of monoclinic VP_2 prepared by ball-milling and annealed. Insets (a) the V polyhedra with 8 P and (b) the VP_2 monoclinic cell.

very badly crystallized VP_2 phase (VP_2-BM). A single annealing of this phase at 600 °C for 4 days in a sealed stainless steel tube followed by air quenching led to a well-crystallized product (Fig. 1). All of the peaks were refined, using a Rietveld method, in a monoclinic cell (SG: C2/m, $a = 8.459(2)$ Å, $b = 3.105(1)$ Å, $c = 7.169(2)$ Å, $\beta = 119.25°$). Interestingly, the parameters of this phase, which will be later on denoted (VP_2-R600), well agree with those referenced in literature (JCPDS-ICDD No. 30–1426, C2/m (12), $a = 8.4641$ Å, $b = 3.1054$ Å, $c = 7.1698$ Å, $\beta = 119.26°$) for the VP_2 obtained by chemical transport technique (using I_2 as the transport agent) [12]. Finally, while not coming as a salient feature on Fig. 1, the baseline shows a large bump centred on $2\Theta = 28°$ suggesting an amorphous component.

The VP_2 crystalline structure, depicted on inset of Fig. 1, presents an $NbAs_2$-type structure. The structure is monoclinic with four V atoms per unit cell occupying the crystallographic positions (4i) V (0.843, 0, 0.302) and 8P atoms on the positions (4i) P1 (0.600, 0,0.400) and P2 (0.141, 0, 0.029). Each V atoms is surrounded by 6 phosphorous atoms in a trigonal prismatic arrangement with two additional phosphorous atoms of neighbouring prisms (a and c directions) capping two tetragonal faces. These bicapped trigonal prisms share their third tetragonal faces forming a V–V bond. To complete the structure, the prisms are stacked along the b direction through their trigonal faces. A projection of the resulting structure on the ac plane is shown in Fig. 1 (inset) with the main interatomic distances. VP_2 has a metallic behaviour [13].

Powders morphologies were investigated by SEM. In both cases shapeless aggregates having an average size ranging from 5 to 30 μm were noted. These aggregates were made of flat and strongly entangled small particles (hundreds of nm), having the VP_2 nominal stoichiometry and being exempt from any metal contamination (from the reactor or the stainless steel tube) as deduced from EDS analysis.

3.2. Electrochemical properties

Two Li/VP_2-BM and Li/VP_2-R600 half-cells were assembled and tested for their electrochemical behaviour (Fig. 2). During the first discharge down to 0 V, the voltage composition curves for VP_2-R600 and VP_2-BM-based Li cells show the insertion of 4.1 and 4.3Li per formula unit, respectively. Upon recharge to 2 V, only 2.7Li per formula unit can be removed from VP_2-R600 and 3.7Li from VP_2-BM leading to reversible capacities of 640 and 890 mAh/g; respectively, the corresponding irreversible capacities being of 37% and 13%, respectively. The two cells exhibit a drastic difference in their capacity retention capabilities. The Li/VP_2-BM cell shows a capacity of 600 mAh/g after 10 cycles at C/5 rate. In contrast, the Li/VP_2-R600 cell rapidly looses its capacity that becomes lower than 200 mAh/g after three cycles only. We inferred such a different behaviour to be correlated to the textural difference between the two samples. Such hypothesis was separately confirmed by measuring better electrochemical performances on 30 min ball-milled VP_2-R600 powders that were showing a featureless X-ray powder pattern.

Another marked difference between the two cells (Fig. 2a) lies in the shape of the first discharge curve. For the Li/VP_2-BM cell, after an initial Li uptake associated to the insertion of Li into the carbon black, the voltage continuously and smoothly decreases to 0 V, as often observed in ball-milled electrodes. This is in deep contrast with the discharge profile of the Li/VP_2-R600 cell that, besides the initial voltage hint associated to carbon black, shows a well-pronounced voltage plateau around 0.2 V. Such a difference, suggesting a different Li reactivity mechanism, is better highlighted in the derivative curves (Fig. 2b), which shows two peaks for the Li/VP_2-R600 cell as opposed to one for Li/VP_2-BM. Once the first discharge is achieved, such a difference is mainly washed out, as the derivative traces for both cells become similar, suggesting that both discharged composites are alike both texturallywise and structurallywise.

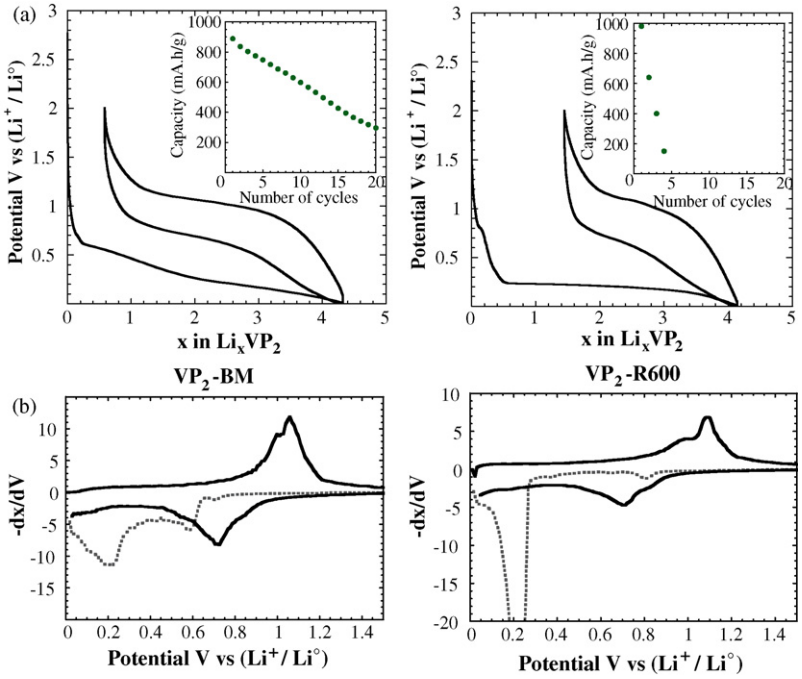

Fig. 2. (a) The voltage-composition curve cell cycled at a C/5 rate between 2 and 0 V together with the corresponding capacity retention for a VP_2-BM/Li (left) and for a VP_2-R600/Li (right); (b) the corresponding incremental capacity for a VP_2-BM/Li (left) and (b) for VP_2-R600/Li (right).

3.3. In situ X-ray diffraction and HRTEM

To grasp more insight into this issue, complementary X-ray diffraction and HRTEM studies were undertaken. Since the VP_2-BM is badly crystallized (Fig. 3a), only the X-ray powder patterns of the fully discharged material was collected. As previously assumed, a full amorphization "from an X-ray point of view" is observed. However, HRTEM study shows a quite different reality: the pristine VP_2-BM material is made of a mixture of many badly crystallized grains and a few 5–10 nm well-crystallized particles (Fig. 3b). At the end of the discharge (Fig. 3c), most of the particles are amorphous while the initially well-crystallized ones are hardly affected by the electrochemical grinding of the reaction (as shown by the arrow locating where the grinding took place). The same general behaviour was recorded during the *in situ* X-ray study of the VP_2-R600 crystalline electrode.

An *in situ* X-ray electrochemical VP_2-R600/Li cell was assembled and discharged at a C/10 rate down to 0 V. X-ray powder patterns were collected for every 0.1 reacted Li, but

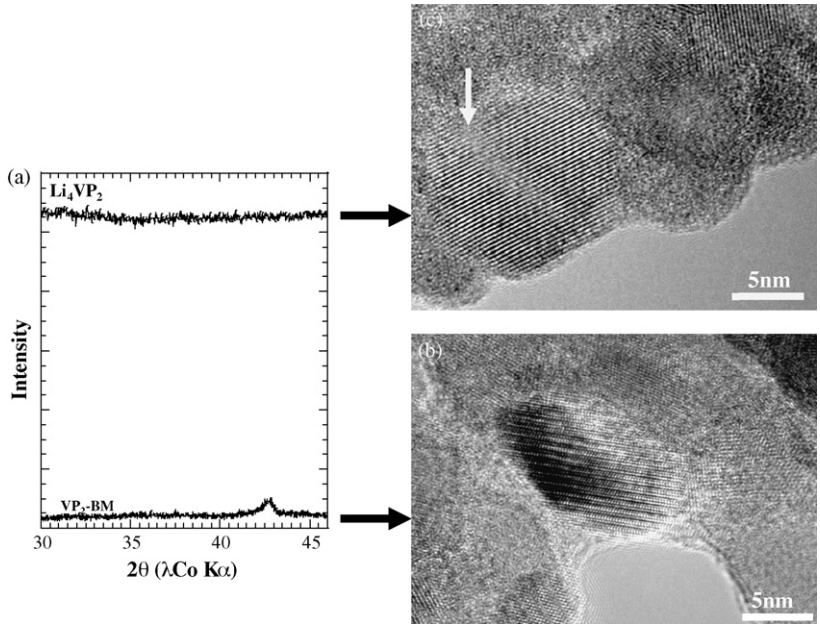

Fig. 3. (a) *In situ* X-ray diffraction patterns for the starting VP_2-BM material (b) and for the VP_2-BM/Li cell (c) cycled until 0.01 V at a C/10 rate.

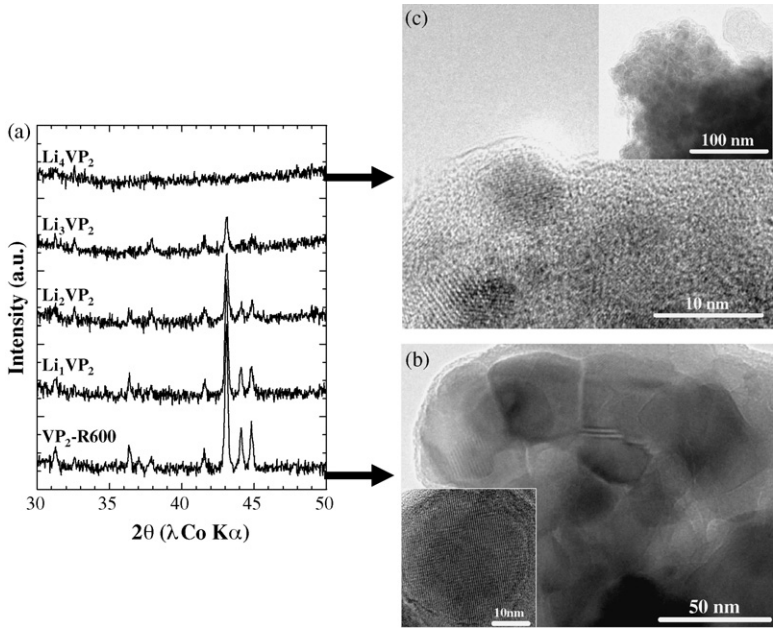

Fig. 4. *In situ* X-ray diffraction patterns for the starting VP_2-R600 material and for the VP_2-R600/Li cell cycled until 0.01 V at a C/10 rate.

only the most relevant ones are reported on Fig. 4a. We note a continuous decrease in the VP_2-R600 main Bragg peaks leading to a featureless X-ray powder pattern reminiscent of a full amorphization. Once the first discharge achieved, the composites were shown to remain amorphous on subsequent charge/discharge as deduced from X-ray monitoring. In neither cases, we observed the presence of any hint of intensity around $2\theta = 50^\circ$ that could have corresponded to the formation of vanadium metal nano-particles.

To further scrutinize this issue an HRTEM study was conducted on the VP_2-R600 electrode prior to being discharged and at the end of the discharge. For the fresh electrode (Fig. 4b), HRTEM reveals a well-crystallized material having the nominal composition VP_2, as deduced from EDS analysis. The major effect of the heat treatment was to increase the material crystallinity and crystallite size by 10 times. Besides, we note the presence of an amorphous layer around the crystallites consistent with our X-ray results. The fully discharged sample is mainly amorphous as indicated by the HRTEM image (Fig. 4c) Nevertheless, we could spot a few remaining crystallized particles corresponding to non-reacted VP_2. No vanadium nanoparticle was observed and it is worth mentioning that EDS spectra realized on amorphous particles do not show any evolution in composition.

To summarize, HRTEM studies indicate that the VP_2 phase (whether crystalline or amorphous) reacts with lithium to form an amorphous "Li_4VP_2" matrix free of V nano-particles and of crystallized Li_3P. In light of such findings we can suppose that the two amorphous phases obtained at the end of discharge for two materials are alike, suggesting that upon subsequent cycles the two samples, whether ball-milled or annealed, behave similarly. To further prove this point, the reduction/oxidation of both materials towards Li was studied in an *ex situ* manner by X-ray atomic absorption spectroscopy.

3.4. Normalized XANES and derivative spectrum

In order to compare quantitatively the intensity of absorption features in various compounds, the experimental K-edge spectra were normalized. The zero energy is taken with respect to the first inflection point of the metal vanadium in the derivative spectrum at 5456.9 eV, which defines the threshold or onset of the photoemission of the 1s electron in vanadium metal. As seen in Fig. 5a, the normalized K-edge XANES spectrum of vanadium metal is characterized by a sharp absorption peak at 1.6 eV, a shoulder at 6.7 eV, followed by a steeply rising edge (the main absorption edge at ~10 eV) that is followed by well-defined peaks at 19.9 and 29.6 eV, and two others at a higher energy in the EXAFS region (not shown here). The normalized K-edge spectra for the VP_2-BM and VP_2-R600 as well as their variation upon Li insertion were identical, so only one is presented. Upon Li insertion, the K-edge XANES spectra for V in the "Li_xVP_2-BM" samples show very little evolution (Fig. 5a), which first indicates that (i) no V metal is produced and (ii) the redox process most likely occurs on the anion site, P or V–P bonds. Such a situation drastically differs from similar XANES measurements performed on NiP_2 upon Li insertion (Fig. 5b). Indeed, the normalized K-edge spectra for Ni in the "Li_xNiP_2" indicates noticeable changes with some evidence of metallic Ni in the fully lithiated "Li_6NiP_2" sample as its K-edge XANES spectrum merges with that of pure Ni. The slight differences observed in the shape of Ni spectrum in Li_6NiP_2 compared to that of Ni sheet can be attributed to size effects. The onset of metallic Ni in the reduced samples was confirmed by EXAFS spectra (Fig. 6b) that clearly show the occurrence of Ni–Ni distances reminiscent of Ni metal in the fully lithiated "Li_6NiP_2" sample, in full agreement with previous HRTEM measurements [6]. For the "Li_xVP_2-BM" system, consistent with the XANES part, EXAFS spectra (Fig. 6a) confirm the absence of notice-

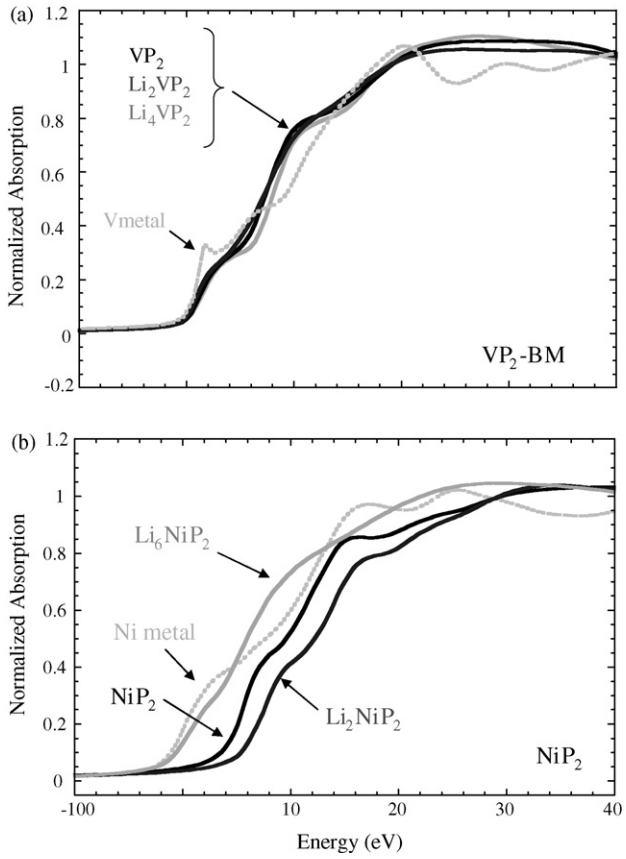

Fig. 5. (a) V K-edge XANES spectra of VP_2-BM compared with (b) Ni K-edge XANES spectra of NiP_2 during the first discharge, in the range of −10 to 40 eV (the zero energy is taken at 5456.9 eV).

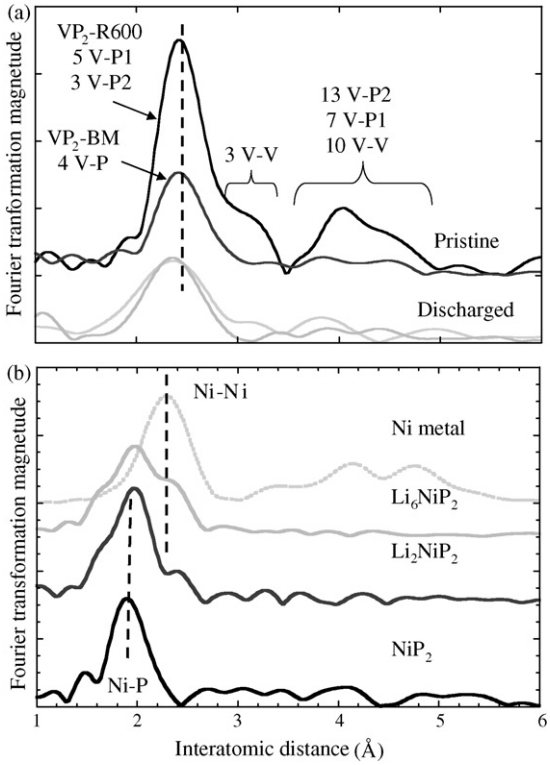

Fig. 6. Pseudoradial distribution functions (not corrected for phase shifts) derived (a) from the EXAFS signals of VP_2-R600, VP_2 on middle discharge (Li_2VP_2), on full discharge (Li_4VP_2), V metal and (b) from the EXAFS signals of NiP_2-monoclinic, NiP_2 on middle discharge (Li_2NiP_2), on full discharge (Li_6NiP_2), Ni metal.

able changes in V, implying that V remains appreciatively in the same state upon Li insertion. It is worth noting however that a difference arises when comparing the EXAFS spectra for the VP_2-R600 and VP_2-BM phases. Upon Li insertion a loss of coordinance is noticed in the case of VP_2-R600 whereas for VP_2-BM the coordinance remains stable. While it is too ambitious to determine a true co-ordination number of V from these spectra, it is nevertheless reasonable to claim that the VP_2-R600 and VP_2-BM samples undergo different structural rearrangements upon their first discharge. Once the first discharge is achieved, the EXAFS spectra for the fully lithiated samples are somewhat identical independently of the nature of the starting phase, *i.e.* crystalline or amorphous. Comparing the NiP_2 and VP_2 electrodes, it appears that the Ni atoms act mainly as the redox centre for the former while it is the "P entities" for the latter as deduced by combined HRTEM, XANES and EXAFS studies.

One remaining question concerns the possibility of having in our fully discharged amorphous "Li_xVP_y" sample the presence of amorphous Li_3P as well. To unambiguously clear such an issue we have conducted both lithium and phosphorous NMR.

Fig. 7 shows the ^{31}P MAS NMR spectrum for a VP_2-R600 electrode discharged to "$Li_{4.5}VP_2$", in comparison with that of the pristine VP_2-R600. The latter shows two phosphorous signals at 566 and 585 ppm (with their spinning sidebands) with similar magnitudes, plus another signal at 289 ppm with smaller magnitude (about 8%) and without spinning sidebands. The two main signals are well consistent with the two expected types of P in the VP_2 structure (4i sites, see Figs. 1 and 2), while the minor one probably comes from an unidentified impurity. The "$Li_{4.5}VP_2$" NMR spectrum shows traces of unreacted VP_2 (with the impurity still present in the same magnitude as in the pristine compound), and a salient signal corresponding to PF_6^- ions from the electrolyte. A negligible amount of Li_3P can be detected at −278 ppm as well as traces of (probably) phosphate species in the vicinity of 0 ppm [14]. Most of the P is actually in a very broad signal around 100 ppm (better seen in the inset), which must originate from a compound exhibiting paramagnetic properties, leading to very strong dipolar interactions on the P nuclei. Although the nature and band structure of the "$Li_{4.5}VP_2$" species are not known, it is not unlikely that reduction can lead to a paramagnetic compound.

Fig. 8 shows the ^7Li MAS NMR signal for the same "$Li_{4.5}VP_2$" from the R600 VP_2 sample. It contains several signals, that cannot be unambiguously assigned at the present time. The main signal (39%) around −0.5 ppm must come from diamagnetic electrolyte or surface reaction type species; the (18%) 3 ppm signal is close to the position of Li_2O, while the others are unknown. Note that for Li_3P, two signals at +0.4 and +4.7 ppm were reported by Tirado et al., none of which is observed here [14].

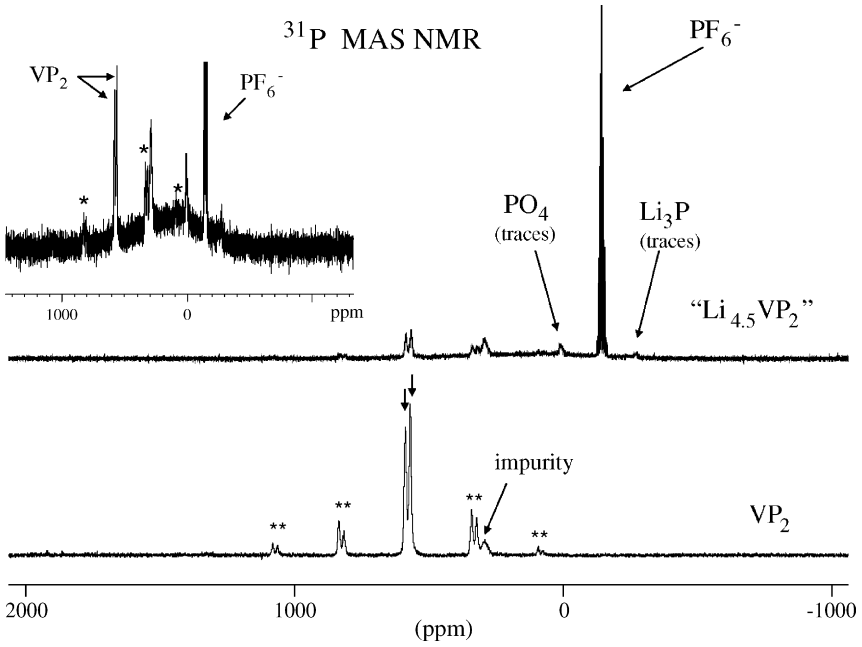

Fig. 7. ^{31}P MAS NMR spectra for VP2 R600 and the discharged "$Li_{4.5}VP_2$" sample (Hahn echo; 30 kHz spinning; ref: H_3PO_4 85%, isotropic signals are shown by arrows and spinning sidebands are marked by *). The spectra are plotted in an absolute scale vs. the mass of sample.

4. Discussion

Vanadium tetraphosphide was recently electrochemically characterized during cycling [15]. A four-step reduction process was proposed: a topotactic insertion in VP_4, a phase transformation into the cubic Li_6VP_4 phase (isostructural of Li_7VP_4 phase), the Li_3P and VP formation by decomposition and another lithium insertion into VP at low potential. Only delithiation of Li_3P occurs to form LiP phase on charge. The first topotactic reduction process was shown to be the only reversible reaction by using a limited potential window.

We reported in this paper the electrochemical reactivity of VP_2 towards Li and experienced several differences with other binary phosphides so far investigated such as (1) a limited range of reacted Li (4 per formula unit as compared to 6 for NiP_2 or FeP_2 for instance), (2) the inability to spot metal particles as previously shown for VP_4, while we have reported evidence of metal nanoparticles in fully reduced CuP_2 and NiP_2 based cells [1,8]. Such results indicate that the mechanism whereby the binary metal phosphide phases react with Li strongly depends on the nature of M. We propose to comment such an observation in light of the large amount of data already existing on the

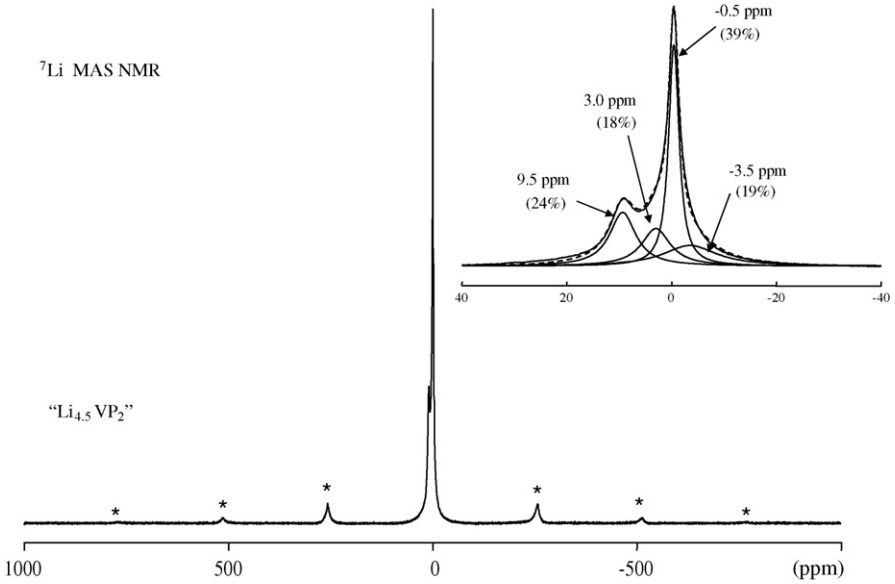

Fig. 8. ^{7}Li MAS NMR spectrum for the "$Li_{4.5}VP_2$" sample (single pulse; 30 kHz spinning; ref: LiCl 1 M; spinning sidebands are marked by *), with a decomposition of the isotropic signal into individual lines.

topic of conversion versus insertion reactions and on the systematic studies of the Li electrochemical reactivity of binary phosphides.

Electrode materials for Li-ion batteries have long been considered as simple redox insertion systems involving one unique atom with either discrete or molecular levels as the redox centre. The arrival of conversion reactions together with the fundamental studies conducted on the electronic structure of the transition metal pnictides Li_xMPn_4 has drastically changed this picture. [3,16,17] In both cases, the amount of reacted Li^+ was found to be greater than one could have expected from transition metal oxidation numbers even by assuming full reduction to a metallic state. For the former, the conversion reaction, the observed extra-capacity (e.g., $2.5Li^+$ per CoO formula unit) was associated to electrolyte decomposition reactions [18]. For the latter, the large number of reversibly exchanged Li^+ (up to $10Li^+$ per formula unit and per transition metal) was explained, using simple concepts of chemical bonding and electron transfers, as due to the $(MPn_4)^{n-}$ anions that were acting as the redox entity. In this respect, the binary MP_x seem to have richer Li electrochemistry since it can either show pure conversion reactions ($CuP_2 \rightarrow Cu + 2Li_3P$ when M = Cu), a coexistence of insertion ($NiP_2 \rightarrow Li_{2.5}NiP_2$) and conversion ($Li_{2.5}NiP_2 \rightarrow Ni + 2Li_3P$) reactions when M is Ni, as compared to a reaction mechanism within which the MP_x anion will act as the redox centre when M = V, Ti. In comparison the Li electrochemical reactivity of binary oxides (MO) is less complicated since we have either conversion reactions for M = Cu, Co, Ni, Fe, Mn, Cr or no reaction at all for M = V or Ti. With sequioxides such as Co_3O_4, Fe_3O_4, the full Li electrochemical reduction involves an insertion reaction ($Fe_2O_3 \rightarrow Li_2Fe_2O_3$) followed by a conversion reaction ($Li_2Fe_2O_3 \rightarrow 2Fe + 3Li_2O$). Whatever the differences between binary oxides or phosphides, it turns out that for both series of compounds the reactivity systematic breaks with V, with for the earlier transition metals absence of reactivity and for the later ones onset of a different reactivity mechanism that is preserved for TiP_2 [19]. Is it purely coincidental or does it bear a meaning? The answer is probably in the electronic band structure showing more covalent M–P bonds for V and Ti phosphides than for the late transition metal phosphide [20].

Let's return to the cyclability of the VP_2 phases that we experienced to be poorer than that measured on the NiP_2 that is far from been excellent by itself. This is due to the limited chemical stability of nanometric Li_3P in the electrolyte that we are presently combating through the uses of electrolyte additives. Interestingly, the electrochemical reactivity of VP_4 was recently shown [15] to react with Li through the following sequence ($VP_4 \rightarrow Li_3VP_4 \rightarrow Li_6VP_4 \rightarrow 9Li_3P + VP$) enlisting insertion and then conversion reactions. We noticed an enhanced capacity retention when the cell was cycled between 0.77 and 2.5 V as compared to a cycling to deeper voltage (0–2.5 V) associated to the appearance/disappearance of Li_3P. Following this line of reasoning, and owing to the absence of Li_3P in the fully reduced "Li_xVP_2" composite samples one would have expected a better cycle life. This is not the case. A possible reason could lie into the Li reactivity mechanism that enlists anionic rather than cationic redox species; therefore, this will have to be proven experimentally through extensive energy electron loss spectroscopy measurements.

5. Conclusion

In short, although all the 3d-metal binary phosphides (M_xP_y) react with Li, it appears that those based on late 3d-transition metals (M = Ni, Co, and Fe) are the most attractive with respect to practical applications since they can reversibly react with at least 6Li per 3d metal or 9 for CoP_3 or NiP_3 [21–23] as compared to solely 4 for VP_2, while showing better capacity retention. Therefore, none of the transition metal so far investigated meets the cycle life criteria to be considered as carbon alternatives. Further work must be directed towards a comprehensive study of the cyclability limitation of phosphides in order to master the electrode/electrolyte stability.

Acknowledgements

The authors would like to thank M.L. Doublet (LSDSMS-Université Montpellier II-France) for helpful discussion. F. G. thanks the "Conseil Régional de Picardie" for its finantial support through a postdoctoral grant. This work was performed in the framework of the Network of Excellence ALISTORE, funded by the European Commission.

References

[1] K. Wang, J. Yang, J. Xie, B. Wang, Z. Wen, Electrochem. Comm. 5 (2003) 480–483.
[2] M.P. Bichat, T. Politova, J.L. Pascal, F. Favier, L. Monconduit, J. Electrochem. Soc. 151 (12) (2004) A2074–A2081.
[3] P. Poizot, S. Laruelle, S. Grugeon, L. Dupont, J.-M. Tarascon, Nature 407 (2000) 496.
[4] J.-M. Tarascon, S. Grugeon, S. Laruelle, D. Larcher, P. Poizot, in: G.A. Nazri, G. Pistoia (Eds.), Lithium Batteries—Science and Technology, Kluwer Academic, Boston, 2003, Chapter 7.
[5] A. Debart, L. Dupont, R. Patrice, J.-M. Tarascon, Solid State Sci. 8 (6) (2006) 640–651.
[6] F. Badway, F. Cosandey, N. Pereira, G.G. Amatucci, J. Electrochem. Soc. 150 (2003) A1318–A1327.
[7] S. Grugeon, S. Laruelle, L. Dupont, J.-M. Tarascon, Solid State Sci. 5 (2003) 895.
[8] F. Gillot, S. Boyanov, L. Dupont, M.-L. Doublet, M. Morcrette, L. Monconduit, J.-M. Tarascon, Chem. Mat. 17 (25) (2005) 6327.
[9] D.C.C. Silva, O. Crosnier, G. Ouvrard, J. Greedan, A. Safa-Sefat, L.F. Nazar, Electrochem. Solid-State Lett. 6 (2003) A162.
[10] S. Denis, E. Baudrin, F. Orsini, G. Ouvrard, M. Touboul, J.-M. Tarascon, J. Power Sources 81/82 (1999) 79–84.
[11] F. Orsini, A. Du Pasquier, B. Beaudoin, J.-M. Tarascon, M. Trentin, E. De Beer, P. Notten, J Power Sources 76 (1998) 19–29.
[12] M. Goelin, B. Carlsson, S. Rundqvist, Acta Chem. Scand. 29 (1975) 706–708.
[13] P. Alemany, S. Alvarez, Inorg. Chem. 31 (1992) 3007–3010.
[14] B. Leon, J.I. Correor, J.L. Tirado, C. Perez-Vicente, J. Electrochem. Soc. 153 (10) (2006) A1829.
[15] Y.U. Kim, B.W. Cho, H.J. Sohn, J. Electrochem. Soc. 152 (8) (2005) A1475–A1478.
[16] M.L. Doublet, F. Lemoigno, F. Gillot, L. Monconduit, Chem. Mat. 14 (10) (2002) 4126.

[17] M.-P. Bichat, F. Gillot, L. Monconduit, F. Favier, M. Morcrette, F. Lemoigno, M.-L. Doublet, Chem. Mat. 16 (6) (2004) 1002–1013.
[18] D. Larcher, G. Sudant, J.B. Leriche, Y. Chabre, J.M. Tarascon, J. Electrochem. Soc. 149 (2002) A234.
[19] S. Woo, H.-J. Sohn, Abs. 264, IMLB 12 Meeting, Electrochem. Soc., 2004.
[20] Doublet M.-L. in preparation, 2007.
[21] R. Alcantara, J.L. Tirado, J.C. Jumas, L. Monconduit, J. Olivier-Fourcade, J. Power Sources 109 (2002) 308.
[22] V. Pralong, D.C.S. Souza, K.T. Leung, L. Nazar, Electrochem. Commun. 4 (6) (2002) 516.
[23] S. Boyanov, F. Gillot, L. Monconduit, J. Power Sources, submitted.